Colloid and Polymer Science
https://doi.org/10.1007/s00396-024-05262-x

RESEARCH

Toward coupling across inorganic/organic hybrid interfaces: polyaniline-coated gold nanoparticles with 4-aminothiophenol as gold-anchoring moieties

Gyusang Yi[1,2,4] · Marisa Hoffmann[1,2,4] · Sezer Seçkin[1,2] · Tobias A. F. König[1,2,3,4] · Ilka Hermes[1] · Christian Rossner[1,2,3] · Andreas Fery[1,2,3,4]

Received: 30 January 2024 / Revised: 26 April 2024 / Accepted: 4 May 2024

Abstract
The chemical binding between metal nanoparticles and (semi-)conductive polymer layers is essential to control the (opto-) electronic properties of such hybrid materials. Current approaches that achieve a conjugated binding of organic (semi-) conductive ligands to metal nanoparticles demonstrated promising functional properties, but are based on tedious multi-step organic synthesis to incorporate the required binding moieties at the chain ends of targeted macromolecular species. Herein, we explore the pre-functionalization of gold nanoparticles with *p*-aminothiophenol and subsequent surfactant-assisted formation of a poly(aniline) (PANI) shell as a means to access gold/PANI core–shell-type nanoparticles with enhanced conductive properties. Controlled surface deposition of these hybrid nanoparticles is achieved via template-assisted self-assembly. For these surface-deposited nanoparticles, charge transport properties are characterized at the nanoscale by conductive atomic force microscopy measurements and show a significant conductivity increase of our core–shell particles as compared to reference particles formed by conventional surfactant-assisted PANI-shell formation.

Keywords Gold nanoparticles · Polyaniline · Hybrid nanomaterials · Surface patterning · Electrically conductive surfaces · Atomic force microscopy

Introduction

Metal nanoparticles feature typical properties of bulk metals such as electrical conductance. Due to this high conductivity, metal nanoparticles can be used for forming conducting elements/ electrodes [1], provided the interparticle gap can be bridged by conducting material [2] or particles can be sintered [3] by post-processing. This established core–shell-type nanoparticles as versatile building blocks in electronic materials. Furthermore, metal nanoparticles feature unique size- and shape-dependent optical properties that derive from their nanoscopic dimensions: The latter results from the resonant excitation of conductance band electrons—confined to the particle surface—by electromagnetic radiation of visible and NIR frequencies, a phenomenon known as localized surface plasmon resonance (LSPR). This LSPR is a very efficient resonant process, oftentimes characterized by extinction cross sections that exceed the geometric cross sections of the metal nanoparticles [4]. The LSPR excitation results in an emergent electromagnetic near-field around the nanoparticles [5]. Concomitantly, the dissipative nature of the excitation leads to heating in the vicinity of the nanoparticles [6, 7], and hot-electron transfer [8] to the environment can occur. Chemical surface modification is key to harnessing these energy transfer processes associated with the LSPR excitation [9]. Therefore, an organic coating layer on the metallic nanoparticle surface opens up opportunities to make use of the confined photonic energy at metal

✉ Andreas Fery
fery@ipfdd.de

1 Institut für Physikalische Chemie und Physik der Polymere, Leibniz-Institut für Polymerforschung Dresden e.V., 01069 Dresden, Germany

2 Faculty of Chemistry and Food Chemistry, Technische Universität Dresden, Bergstraße 66, 01069 Dresden, Germany

3 Dresden Center for Intelligent Materials (DCIM), Technische Universität Dresden, Hallwachsstraße 3, 01069 Dresden, Germany

4 Center for Advancing Electronics Dresden (Cfaed), Technische Universität Dresden, Helmholtzstraße 18, 01069 Dresden, Germany

Published online: 15 May 2024

nanoparticles. Such coating layer additionally provides "soft" properties, by which it is possible to equip hybrid colloids with structural plasticity [10] and/or additional functional properties [11], e.g., photo response [12]. The polymeric coating layer can also be used to mediate the self-assembly of AuNPs into supracolloidal structures [12–14]. As a result of the described possibilities, such hybrid metal/organic core–shell-type colloids are versatile building blocks in forming materials with optical [15] and/or electronic functionality [2].

One prototype example in this context is the combination of gold-nanoparticle cores with polyaniline (PANI) shells [16–20]. While the gold core provides the mentioned conductive as well as plasmonic properties, the PANI shell acts as a redox-[16, 17, 19] and pH-switchable [17, 18, 20] surface coating, which is electrically conductive in its protonated or doped state [21]. The photochromic behavior of the PANI coating layer in conjuncture with the plasmonic properties of the core led to the realization of, e.g., plasmonic switches [18, 19]. Controlled surface deposition of these core–shell-type particles was used to create switchable plasmonic metasurfaces with anti-reflective [22] and holographic capability [23]. For such hybrid metal/organic-semiconductor nanocomposite materials, the connection between both elements can be critical because charge transfer between the metallic core and a (semi-)conducting polymer layer may strongly affect the (opto-)electronic properties of derived materials and devices [24]. For those reasons, the chemistry of the interface between metal nanoparticles and (semi-)conductive polymer shells is of vast contemporary interest. New synthetic strategies to exert control in this domain are currently under development [25–27]; however, the required multi-step organic synthesis impedes the large-scale application of these promising nanomaterials.

Our contribution is motivated by the need for electronic communication through the interface in metal/(semi-)conducting polymer core–shell nanoparticles. Building on this motivation, we study the applicability of a strategy [28, 29] developed for coating flat bulk gold surfaces with polyaniline (PANI) for coating gold nanoparticles. This strategy involved pre-adsorption of *p*-aminothiophenol (pATP) prior to forming the PANI film. After PANI-film formation on gold electrodes, faster discharge kinetics were observed in the case of pATP pre-adsorption prior to PANI deposition compared with direct PANI deposition, suggesting improved charge transfer through the interface in the former scenario. Thus, in this work, we aimed to implement pATP pre-adsorption into established, surfactant-based wet-chemical strategies [30, 31] as a means for coating gold nanoparticles with PANI shells in a conjugated manner (see Scheme 1 for an illustration of the synthetic strategy). We confirmed the improved electronic communication of the prepared core–shell-type nanoparticles by conductive atomic force microscopy (cAFM) measurements.

Materials and methods

Materials

Hexadecyltrimethylammonium chloride (CTAC, 25 wt% in H_2O), L-(+)-ascorbic acid (AA, > 99%), sodium borohydride ($NaBH_4$, 99%), sodium dodecyl sulfate (SDS, > 99%), and aniline (> 99%) were obtained from Sigma-Aldrich. Hydrogen tetrachloroaurate trihydrate ($HAuCl_4 \cdot 3H_2O$, 99.99%) was purchased from abcr GmbH. Hydrochloric acid (AnalaR Normapur®, 37%) was obtained from VWR Chemicals. Hexadecyltrimethylammonium bromide (CTAB, 99%) was purchased from Merck KGaA. Sylgard 184 PDMS elastomer kits were obtained from Dow Corning. All materials were used as obtained. Purified Milli-Q-grade water (18.2 MΩ·cm, pH 8) was used in all experiments. Cr and Au for evaporation were purchased from Kurt J. Lesker company, USA. Si wafers (p-type, boron dopant, 1–20 Ω·cm) were obtained from CrysTec KRISTALLTECHNOLOGIE.

Synthesis

For the synthesis of spherical gold nanoparticle, the seed-mediated growth method [32] was adapted.

Au seed synthesis (2 nm). Aqueous CTAB solution (0.1 M, 4.7 mL) was kept at 32 ℃ and mixed with $HAuCl_4$ solution (0.05 M, 25 µL). The mixture was stirred at high speed, and $NaBH_4$ (0.01 M, 300 µL) was quickly added. Rapid stirring was continued for 30 s and the stirring speed was changed to 300 rpm, at which stirring proceeded for 30 min at 32 ℃. During the reaction, the color of the solution changed to brownish color.

Au seed synthesis (8 nm). Aqueous hexadecyltrimethylammonium chloride (CTAC, 0.2 M, 40 mL), aqueous L-(+)-ascorbic acid (0.1 M, 30 mL), 1 mL of the 2 nm seed solution, and $HAuCl_4$ solution (0.5 mM, 40 mL) were mixed and stirred for 15 min at 300 rpm. After that, two centrifugation/re-dispersion cycles were performed: 15,000 rcf, 1 h; re-dispersion in aqueous CTAC solution (0.02 M, 10 mL).

Nanoparticle synthesis (Au@CTAC 50 nm). An aqueous solution of L-(+)-ascorbic acid (AA) and CTAC (AA: 1.3 mM, CTAC: 60 mM, 200 mL) was prepared. Then, a solution of 8 nm seeds (840 µL) was added while stirring at 380 rpm.

In another vessel, the growth solution ($HAuCl_4$: 1 mM and CTAC: 60 mM, 200 mL) was prepared and warmed at 45 ℃. This solution was divided into three 60 mL syringes and slowly dropwise added to the 8 nm seed solution (0.5 mL/min) by a syringe pump. After slow addition by syringes, the remaining 20 mL of growth solution was poured in for etching to obtain spherical particles and mixed for additional 15 min. The final product was centrifuged to 2000 rcf twice, 20 min each, and re-dispersed in CTAC (0.01 M, 30 mL).

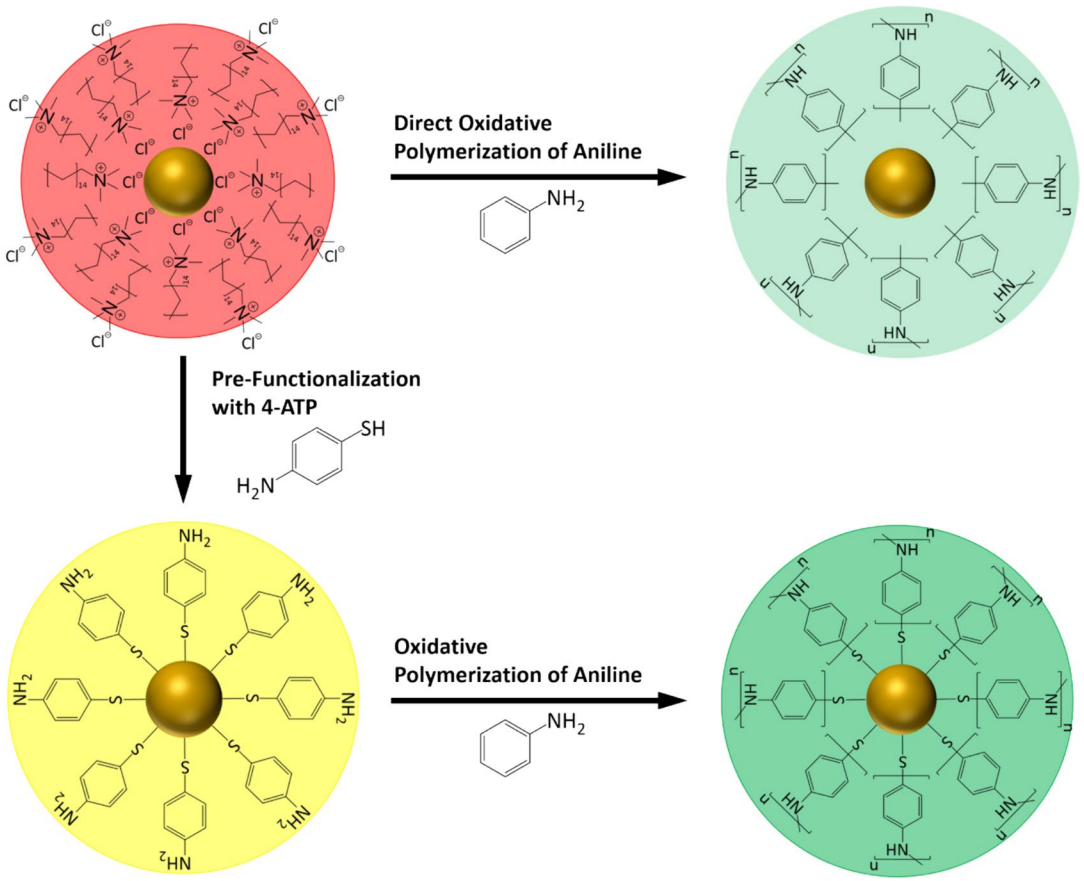

Scheme 1 Top: Direct oxidative polymerization of aniline at surfactant (CTAC)-coated gold nanoparticles. Bottom: Pre-functionalization of the gold surface with 4-aminothiophenol and subsequent oxidative polymerization of aniline

Functionalization of gold nanoparticles with 4-aminothiophenol (Au@ATP). A method from Üzer et al. [33] was adapted. 800 µL of Au@CTAC solution was mixed with HCl (1 M, 0.8 µL) for adjusting pH at 3 and stirred at 350 rpm at 60 ℃ (heating plate). Ethanolic solution of 4-ATP (0.41 mM, 100 µL) was added, and stirring continued for 3 h. Centrifugation was not conducted since the 4-amniothiophenol functionalized particles had a propensity for aggregation during centrifugation.

Oxidative polymerization of aniline. The surfactant-assisted oxidative polymerization process was adapted for the synthesis of polyaniline shells [34]. Au@CTAC or Au@ATP (0.5 mg/mL, 500 µL) were prepared. Milli-Q-grade water (2252 µL), SDS (80 mM, 219 µL), HCl (1 M, 15 µL), aniline (10 mM, 300 µL), and APS (13.33 mM, 375 µL) were added to the particles in this order while stirring vigorously. The solution was stirred at 900 rpm for 1 h. After that, the stirring speed was changed to 130 rpm. Eventually, the solution color changed to green (Au@CTAC for 7 h and Au@ATP for 18 h).

Thermal evaporation of metal films

Si wafers were cleaned successively by acetone and ethanol sonication each for 5 min. The wafers were mounted onto a substrate holder for a PVD (physical vapor deposition) chamber (Hex, Korvus Technology). A 5 nm layer of chromium was deposited as an adhesion layer with a deposition rate of 0.5 Å/s, and on the top of the Cr layer, 30 nm of Au was deposited with 0.3 Å/s. During that process, the substrates were rotated at 15 rpm to maintain homogeneity of deposition across the sample. The obtained Au/Cr/Si wafers were used as substrates for conductive AFM measurements.

Template fabrication

The method for template fabrication was adapted from previous work [32]. Cross-linker (4.58 g) and prepolymer (22.92 g) from the Sylgard kit were mixed for 1:5 (cross-linker to prepolymer) ratio PDMS. The mixture was poured into a leveled square polystyrene dish. The mixture was

cured at 80 ℃ for 5 h and kept at room temperature overnight. PDMS was cut into 1 × 4.5 cm^2 strips. The strips were elongated by 40% with a stretching device. The stretched PDMS strips were treated with oxygen plasma (80 W, 90 s) at a pressure of 0.3 mbar. After plasma treatment, the strips were cooled to room temperature and relaxed from the strain. The wrinkled PDMS was cut into pieces of 1 × 1 cm^2 and cleaned with distilled water.

Nanoparticle assembly

Template-assisted assembly was performed via spin-coating on wrinkled substrates [32]. The wrinkled templates were hydrophilized in oxygen plasma (80 W, 45 s, 0.2 mbar). A gold-nanoparticle solution (4 µL, 10 mg/mL) was cast onto the hydrophilized PDMS templates. The spin-coating was done in a two-step manner (first: 222 rpm for 2 s; second: 1700 rpm for 90 s; photoresist spinner, Headway Research Inc.).

Au/Cr/Si wafers were cleaned successively with acetone and ethanol, each with 5 min of sonication. The substrates were hydrophilized in oxygen plasma with 80 W for 180 s at a pressure of 0.2 mbar. 10 µL of Milli-Q-grade water was spread onto the hydrophilized substrates, and the particle-filled PDMS were stamped onto the substrates for 6 h to transfer the particle assembly to the Au/Cr/Si substrate.

Visible/NIR extinction spectroscopy

A Cary 5000 spectrometer (Agilent, USA) was used for extinction spectroscopy. The measurement was performed in the range of 400 to 1000 nm (scan rate, 600 nm/min). A fixed 3 × 4 mm^2 spot size was used.

Transmission electron microscopy (TEM)

TEM images were obtained using a Libra 120 (Zeiss, Germany). Measurements were performed at an acceleration voltage of 120 kV. Analyte samples were diluted to approx. 0.1 mg/mL of gold nanoparticles with Milli-Q-grade water, and 5.5 µL of such solution was dried overnight on CF200-Cu-50 TEM grids (carbon support film on 200 mesh copper, Electron Microscopy Sciences, USA). The images were analyzed using ImageJ software.

Surface-enhanced Raman scattering (SERS)

Surface-enhanced Raman spectroscopy (SERS) measurements were conducted by a Renishaw inVia Qontor confocal Raman spectrometer with backscattering configuration (Gloucestershire, UK). The Leica microscope with a lens of × 20 magnification and NA 0.45 (Leica Microsystems GmbH Wetzlar, Germany) was operated. Samples were excited by a laser with 633 nm wavelength with the constant laser power at 290 µW, and the acquisition time was set to 15 s. The acquired Raman signals were dispersed through a grating with 1800 l/mm and recorded by a CCD detector.

Conductive AFM

Conductive AFM experiments were performed on a Bruker Icon AFM in Peak force Tuna mode. An ElectriMulti75-G-10 cantilever (3 N/m, 75 kHz, coated by 5 nm Cr and 25 nm Pt, BudgetSensors) was used. The conductive substrate (Au/Cr film on Si wafer) was electrically connected to the AFM sample bias line by conductive copper tape. Measurements were conducted in the bias range from − 200 to 200 mV in 50 mV steps. The obtained data were processed by Gwyddion software[35]. From the height profiles of the image, the particle assemblies were masked, and the median current of the masked area was calculated. The current value comparison of different samples was conducted with the same cantilever.

Results and discussion

The gold nanoparticles used in this work were prepared by the seeded growth method (see the "Materials and methods" section) and originally obtained with a hexadecyltrimethylammonium chloride (CTAC) bilayer in aqueous solution comprising gold cores with an average diameter of 51.5 ± 2.3 nm, as determined by TEM measurements. In a subsequent step, the pre-functionalization of these particles with 4-aminothiophenol was undertaken at acidic pH, following a strategy already reported elsewhere [33]. The surface chemistry of both the original, CTAC-coated gold nanoparticles (Au@CTAC) and also the pre-functionalized gold nanoparticles (Au@ATP) were investigated by Raman spectroscopy (Fig. 1a). From those experiments, a pronounced peak at approx. 275 cm^{-1} that can be assigned to the Cl-Au stretching vibration [36] was observed for Au@CTAC nanoparticles (red trace in Fig. 1a), indicative of chemisorbed Cl^- at the gold surface, which confines the CTAC surfactant to the gold surface. After the described pre-functionalization with 4-aminothiophenol, a decreased intensity of this peak ascribed to the excitation of the Cl-Au stretching vibration is noticed; on the other hand, a previously not observed peak at approx. 1077 cm^{-1} is noticed, which is assigned to the C-S stretching vibration of 4-aminothiophenol [37]. The C–C stretching vibration of 4-aminothiophenol (1586 cm^{-1}) is also observed in a longer wavenumber region (Fig. S1) [37]. Thus, these Raman experiments strongly suggest a replacement of the majority of CTAC surfactant at the gold-nanoparticle surface with the competitive ligand 4-aminothiophenol. Fully in line with this ligand substitution reaction at the surface is a very minor change in the plasmon resonance peak of the gold nanoparticles (Fig. 1b).

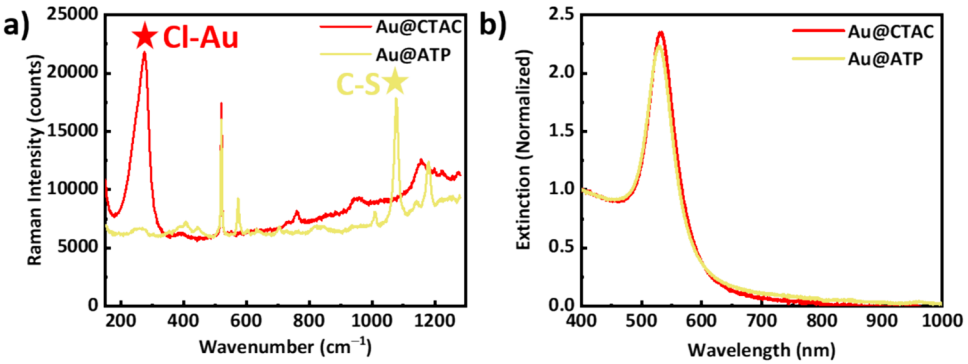

Fig. 1 **a** Raman spectra for initial CTAC-coated gold nanoparticles (red trace) and gold nanoparticles functionalized with 4-aminothiophenol (yellow trace). **b** Extinction spectra (normalized to 1.0 at 400 nm wavelength) for initial CTAC-coated gold nanoparticles (red trace) and gold nanoparticles functionalized with 4-aminothiophenol (yellow trace)

The spectra in Fig. 1b are normalized to their extinction at 400 nm, at which extinction stems mainly from interband transitions within gold, which is, therefore, a normalization with respect to total gold content [38]. The slight resonance wavelength shift (from 533 nm before to 530 nm after functionalization with pATP) can be attributed to a change of the refractive index around the gold nanoparticle [39], while the overall linewidth of the resonance remains unaffected. This result indicated that the gold nanoparticles remained dispersed as individual entities in the solution; thus, colloidal stability was not compromised after this pre-functionalization.

In the next step, core–shell-type nanoparticles were prepared through oxidative polymerization from aniline starting from the different precursors: Au@CTAC and Au@ATP (Scheme 1). In this reaction, sodium dodecyl sulfate (SDS) micelles are mixed with aniline monomer to form aniline-inserted SDS micelles. The micelles are negatively charged and interact electrostatically with positively charged CTAC-stabilized gold nanoparticles (Au@CTAC) [34] or the positive charges supported by the primary amine groups present in 4-ATP-functionalized gold nanoparticles (Au@ATP). During the oxidative polymerization at Au@ATP particles, PANI shells can be initiated from or terminated at the surface-immobilized 4-ATP [29]. The polymerization resulted in PANI shells on both kinds of gold nanoparticles, which had slightly different but comparable shell thicknesses, as determined from TEM images (i.e., 12.6 ± 2.2 nm for Au@ATP-PANI and 14.7 ± 2.6 nm for Au@PANI; see Fig. 2a, b for exemplary transmission electron microscopy images and supporting information Fig. S2 for shell-thickness distributions). The formation of the PANI shell is also evident from Raman experiments (pronounced peaks at approx. 1179, 1344, 1514, and 1599 cm^{-1} for Au@ATP-PANI and 1174, 1343, 1513, and 1593 cm^{-1} for Au@PANI) (Fig. 2c) [40]. These Raman measurements furthermore showed that the signal characteristic of the C-S stretch remained for the measurements conducted at the Au@ATP-PANI sample [37]. We can thus conclude that 4-ATP is not replaced during the oxidative polymerization but remains anchored at the gold nanoparticle surface after the PANI-shell formation. Visible/NIR extinction spectra for both core–shell-type nanohybrids are displayed in Fig. 2d. The excitation of the plasmon resonance occurs with a comparably narrow linewidth for both cases, again indicating the good dispersion in the colloidal solution state. In addition, the broad absorbance centered around approx. 830 nm and toward smaller wavelength (at the high-energy shoulder of the LSPR peak) can be attributed to PANI in its protonated state [17]. Because of the absorbance of PANI also at 400 nm, no normalization of the spectra to total gold content as done in Fig. 1b could be performed here. LSPR peak maxima show a red shift after oxidative polymerization from Au@ATP (530 nm) to Au@ATP-PANI (541 nm) and from Au@CTAC (533 nm) to Au@PANI (536 nm). The larger red shift of Au@ATP-PANI is shown compared to Au@PANI. Also, the more substantial PANI

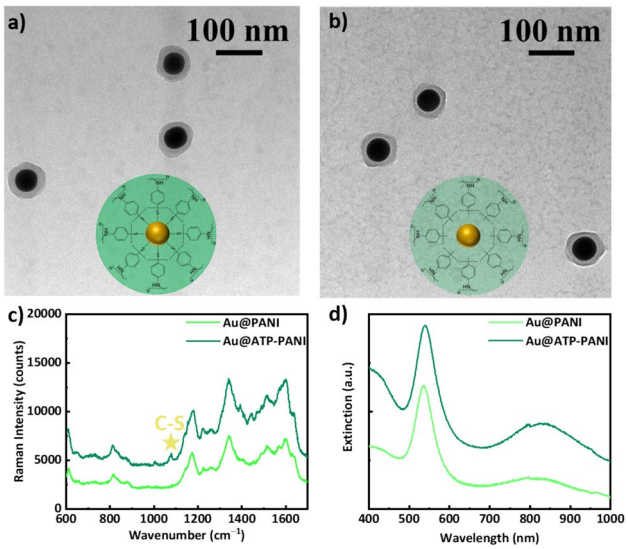

Fig. 2 Bright-field transmission electron micrographs of **a** Au@ATP-PANI and **b** Au@PANI. **c** Raman spectra of both hybrid nanoparticles. **d** Visible/NIR extinction spectra of both hybrid nanoparticles, revealing the localized surface plasmon resonance of the golden cores at approx. 530 nm, while the broad absorbance centered around approx. 830 nm can be attributed to PANI in its protonated state

absorbance in the case of the Au@ATP-PANI particles compared with the Au@PANI particle can partly be explained by the slightly thicker polymer layers in the former sample. However, it could also result from electronic coupling to the gold-nanoparticle core within the Au@ATP-PANI sample. Thus, we performed conductive AFM experiments in the next step to investigate such possible electronic coupling between the gold core and the PANI shell.

For AFM measurements, we prepared hybrid nanoparticle assemblies on the conducting substrates (Au/Cr/Si wafer) serving as back electrodes (see above in the Experimental section). The currents of assemblies were resolved in a bias range from − 200 to 200 mV. AFM topography and corresponding current image for the 200 mV scan are shown in Fig. 3.

Both particle assemblies featured a clear current response upon bias application. However, where the Au@ATP-PANI particle assembly gave a median current of 53 pA, the Au@PANI assembly featured a median current of only 1 pA, illustrating the distinct difference in conductivity for both particles (this is substantiated by a more complete data set presented in the supporting information). The higher current signal on Au@ATP-PANI suggests an improved electronic coupling between the polymer shell and the metal core. The limited substrate conductivity surrounding the particle assembly likely originates from organic residue following deposition.

The average diameter of the particles was determined from AFM topography line profiles across individual particles via the full width at half maximum (FWHM) of a Gaussian fit (Fig. S3–S4). For Au@ATP-PANI, the diameter from FWHM is 107.2 ± 6.2 nm, and the average diameter of Au@PANI from FWHM is 106.9 ± 7.9 nm. Confirming our previous observations from TEM measurements, the ATP layer increases the particle dimensions only slightly. The larger absolute values from AFM compared to those determined from TEM (79.5 ± 4.4 nm for Au@ATP-PANI and 77.4 ± 4.6 nm for Au@PANI) can be attributed to the tip-sample convolution from the AFM tip radius, which is given with nominal value of 25 nm. The distribution of diameters from TEM is shown in Fig. S5.

The median currents of the particle-line assemblies are plotted for biases in the range of − 200 to 200 mV (Fig. 4). Corresponding topography and current images are shown in Fig. S6–S7. Over the entire bias range, the current of Au@ATP-PANI is consistently larger than that of Au@PANI confirming that the pre-functionalization of the gold nanoparticles with p-ATP improves the electronic coupling between gold cores and PANI shells so the gold core can contribute to the conductivity of particles. Due to the lack of linkers between the gold core and PANI shells in Au@PANI, the electrical contribution from the gold core is strongly reduced, and the particles' conductivity mainly stems from

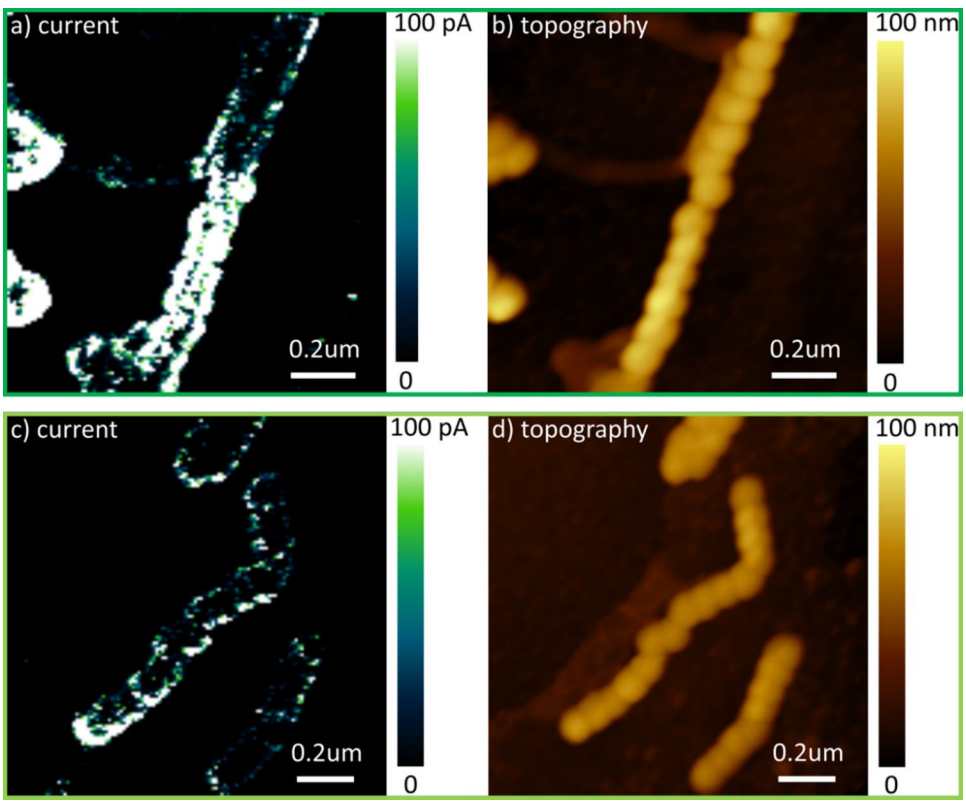

Fig. 3 cAFM current image and corresponding topography **a** current of Au@ATP-PANI, **b** topography of Au@ATP-PANI, **c** current of Au@PANI, and **d** topography of Au@PANI (same cantilever used)

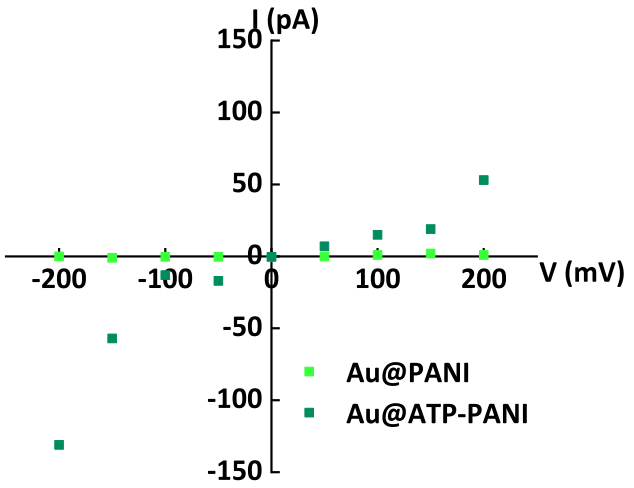

Fig. 4 Median current of Au@PANI (light green) and Au@ATP-PANI (dark green) as a function of the bias voltage (−200 ~ 200 mV) (same cantilever used in Fig. 3)

the PANI shell. I-V characteristics of both assemblies appear to feature a slight s-shape, suggesting a non-ohmic behavior, with a rapidly increasing current value at higher voltages of 200 and − 200 mV, similar to the I-V curve of PANI [41, 42]. This I-V curve shape indicates semiconductor contribution to the materials' conductivity, thus implying that, even though the influence of the gold core on the conductivity is increased, the PANI shell still affects the charge transport mechanism of the Au@ATP-PANI. Additional measurements of conductive AFM corroborate the reported trends and are shown in the supporting information (Fig. S8–S10).

Conclusion

We established a straightforward strategy for coupling polyaniline shells to gold nanoparticles that improved the electrical conductivity of the formed hybrid core–shell-type nanoparticle, as evidenced by c-AFM measurements. Our approach is based on the pre-functionalization of the golden nanoparticles with "off-the-shelf" 4-aminothiophenol prior to the polyaniline-shell formation, enabling an efficient and straightforward synthetic procedure. In particular, in conjunction with the presented template-assisted line-assembly approach, these core–shell-type nanoparticles have potential for creating surfaces with anisotropic conductance [43]. At the same time, the responsive nature of the polymer shell provides prospects for sensor development or on-demand modulation of charge transport properties by specific external stimuli such as pH, in addition to more unspecific external factors, such as bending or strain [44]. Therefore, our approach provides tempting prospects for next-generation electronic materials.

Supplementary Information The online version contains supplementary material available at https://doi.org/10.1007/s00396-024-05262-x.

Acknowledgements The authors acknowledge Yudhajit Bhattacharje for performing the vapor deposition. This work was supported by the Deutsche Forschungsgemeinschaft (DFG, German Research Foundation) – GRK 2767 – Projektnummer 451785257. We acknowledge financial support from Leibniz-Kooperative Exzellenz project K524/2023. The Volkswagen Foundation financially supported this project through a Freigeist Fellowship to T.A.F.K. C.R. acknowledges receipt of a Liebig fellowship (Fonds der Chemischen Industrie).

Author contribution Conceptualization: C.R. and A.F.; methodology: G.Y., M.H., S.S., I.H. Formal analysis: G.Y., M.H., S.S., I.H. Investigation: G.Y., M.H., S.S., I.H. Data curation: G.Y., S.S. writing—original draft preparation: G.Y., I.H., C.R. writing—review and editing: G.Y., M.H., S.S., T.A.F.K., I.H., C.R., A.F. visualization: G.Y., I.H. supervision: T.A.F.K., C.R., A.F.; funding acquisition: T.A.F.K., I.H., C.R., A.F. All authors have read and agreed to the published version of the manuscript.

Funding Open Access funding enabled and organized by Projekt DEAL. This work was supported by the Deutsche Forschungsgemeinschaft (DFG, German Research Foundation)–GRK 2767–Projektnummer 451785257. We acknowledge financial support from Leibniz-Kooperative Exzellenz project K524/2023. The Volkswagen Foundation financially supported this project through a Freigeist Fellowship to T.A.F.K. C.R. acknowledges receipt of a Liebig fellowship (Fonds der Chemischen Industrie).

Data availability Data is provided within the manuscript or supplementary information files.

Declarations

Ethical approval Does not apply.

Competing interest The authors declare no competing interests.

References

1. Kister T, Maurer JHM, González-García L, Kraus T (2018) Ligand-dependent nanoparticle assembly and its impact on the printing of transparent electrodes. ACS Appl Mater Interfaces 10(7):6079–6083. https://doi.org/10.1021/acsami.7b18579
2. Reiser B, González-García L, Kanelidis I, Maurer JHM, Kraus T (2016) Gold nanorods with conjugated polymer ligands: sintering-free conductive inks for printed electronics. Chem Sci 7(7):4190–4196. https://doi.org/10.1039/c6sc00142d

3. Grouchko M, Kamyshny A, Mihailescu CF, Anghel DF, Magdassi S (2011) Conductive inks with a "built-in" mechanism that enables sintering at room temperature. ACS Nano 5(4):3354–3359. https://doi.org/10.1021/nn2005848
4. Garcia MA (2011) Surface plasmons in metallic nanoparticles: fundamentals and applications. J Phys D Appl Phys 44(28). https://doi.org/10.1088/0022-3727/44/28/283001
5. Kelly KL, Coronado E, Zhao LL, Schatz GC (2003) The optical properties of metal nanoparticles: the influence of size, shape, and dielectric environment. J Phys Chem B 107(3):668–677. https://doi.org/10.1021/jp026731y
6. Yashchenok A, Masic A, Gorin D, Inozemtseva O, Shim BS, Kotov N, Skirtach A, Möhwald H (2015) Optical heating and temperature determination of core-shell gold nanoparticles and single-walled carbon nanotube microparticles. Small 11(11):1320–1327. https://doi.org/10.1002/smll.201401697
7. Manrique-Bedoya S, Abdul-Moqueet M, Lopez P, Gray T, Disiena M, Locker A, Kwee S, Tang L, Hood RL, Feng Y, Large N, Mayer KM (2020) Multiphysics modeling of plasmonic photothermal heating effects in gold nanoparticles and nanoparticle arrays. J Phys Chem C 124(31):17172–17182. https://doi.org/10.1021/acs.jpcc.0c02443
8. Primo A, Corma A, García H (2011) Titania supported gold nanoparticles as photocatalyst. Phys Chem Chem Phys 13(3):886–910. https://doi.org/10.1039/C0CP00917B
9. Rossner C, König TAF, Fery A (2023) Hairy plasmonic nanoparticles. In Hairy nanoparticles - from synthesis to applications; Lin, Z., Liu, Y., Eds.; Wiley-VCH, 351–374
10. Rossner C, Letofsky-Papst I, Fery A, Lederer A, Kothleitner G (2018) Thermoreversible surface polymer patches: a cryogenic transmission electron microscopy investigation. Langmuir 34(29):8622–8628. https://doi.org/10.1021/acs.langmuir.8b01742
11. Gibson MI, Danial M, Klok HA (2011) Sequentially modified, polymer-stabilized gold nanoparticle libraries: convergent synthesis and aggregation behavior. ACS Comb Sci 13(3):286–297. https://doi.org/10.1021/co100099r
12. Huebner D, Rossner C, Vana P (2016) Light-induced self-assembly of gold nanoparticles with a photoresponsive polymer shell. Polymer 107:503–508. https://doi.org/10.1016/j.polymer.2016.05.073
13. Coelho JP, Tardajos G, Stepanenko V, Roedle A, Fernández G, Martínez AG (2015) Cooperative self-assembly transfer from hierarchical supramolecular polymers to gold nanoparticles. ACS Nano 9:11241. https://doi.org/10.1021/acsnano.5b04841
14. Coelho JP, Rubio GG, Delices A, Barcina JO, Salgado C, Ávila D, Rodríguez OP, Tardajos G, Martínez AG (2014) Polyrotaxane-mediated self-assembly of gold nanospheres into fully reversible supercrystals. Angew Chem Int Ed 53:12751. https://doi.org/10.1002/anie.201406323
15. Probst PT, Mayer M, Gupta V, Steiner AM, Zhou Z, Auernhammer GK, König TAF, Fery A (2021) Mechano-tunable chiral metasurfaces via colloidal assembly. Nat Mater 20:1024–1028. https://doi.org/10.1038/s41563-021-00991-8
16. Jeon JW, Ledin PA, Geldmeier JA, Ponder JF, Mahmoud MA, El-Sayed M, Reynolds JR, Tsukruk VV (2016) Electrically controlled plasmonic behavior of gold nanocube@polyaniline nanostructures: transparent plasmonic aggregates. Chem Mater 28(8):2868–2881. https://doi.org/10.1021/acs.chemmater.6b00882
17. Jeon JW, Zhou J, Geldmeier JA, Ponder JF, Mahmoud MA, El-Sayed M, Reynolds JR, Tsukruk VV (2016) Dual-responsive reversible plasmonic behavior of core-shell nanostructures with PH-sensitive and electroactive polymer shells. Chem Mater 28(20):7551–7563. https://doi.org/10.1021/acs.chemmater.6b04026
18. Jiang N, Shao L, Wang J (2014) (Gold nanorod core)/(polyaniline shell) plasmonic switches with large plasmon shifts and modulation depths. Adv Mater 26(20):3282–3289. https://doi.org/10.1002/adma.201305905
19. Lu W, Jiang N, Wang J (2017) Active electrochemical plasmonic switching on polyaniline-coated gold nanocrystals. Adv Mater 29(8):1604862. https://doi.org/10.1002/adma.201604862
20. Jones A, Searles EK, Mayer M, Hoffmann M, Gross N, Oh H, Fery A, Link S, Landes CF (2023) Active control of energy transfer in plasmonic nanorod-polyaniline hybrids. J Phys Chem Lett 14(36):8235–8243. https://doi.org/10.1021/acs.jpclett.3c01990
21. Chiang JC, MacDiarmid AG (1986) "Polyaniline": protonic acid doping of the emeraldine form to the metallic regime. Synth Met 13(1–3):193–205. https://doi.org/10.1016/0379-6779(86)90070-6
22. Brasse Y, Ng C, Magnozzi M, Zhang H, Mulvaney P, Fery A, Gómez DE (2020) A tunable polymer–metal based anti-reflective metasurface. Macromol Rapid Commun 41(1):1900415. https://doi.org/10.1002/marc.201900415
23. Kaissner R, Li J, Lu W, Li X, Neubrech F, Wang J, Liu N (2021) Electrochemically controlled metasurfaces with high-contrast switching at visible frequencies. Sci Adv 7(19):eabd9450. https://doi.org/10.1126/sciadv.abd9450
24. Steiner AM, Lissel F, Fery A, Lauth J, Scheele M (2021) Prospects of coupled organic–inorganic nanostructures for charge and energy transfer applications. Angewandte Chemie - International Edition 60(3):1152–1175. https://doi.org/10.1002/anie.201916402
25. Delabie J, De Winter J, Deschaume O, Bartic C, Gerbaux P, Verbiest T, Koeckelberghs G (2020) Development of a layered hybrid nanocomposite material using α, ω-bifunctionalized polythiophenes. Macromolecules 53(24):11098–11105. https://doi.org/10.1021/acs.macromol.0c01593
26. Delabie J, Ceunen W, Detavernier S, De Winter J, Gerbaux P, Verbiest T, Koeckelberghs G (2021) Catechol as a universal linker for the synthesis of hybrid polyfluorene/nanoparticle materials. Macromolecules 54(10):4582–4591. https://doi.org/10.1021/acs.macromol.1c00386
27. Sun N, Zhang ST, Simon F, Steiner AM, Schubert J, Du Y, Qiao Z, Fery A, Lissel F (2021) Poly(3-hexylthiophene)s functionalized with n-heterocyclic carbenes as robust and conductive ligands for the stabilization of gold nanoparticles. Angewandte Chemie - International Edition 60(8):3912–3917. https://doi.org/10.1002/anie.202012216
28. Rubinstein I, Rishpon J, Sabatani E, Redondo A, Gottesfeld S (1990) Morphology control in electrochemically grown conducting polymer films. 1. Precoating the metal substrate with an organic monolayer. J Am Chem Soc 112(16):6135–6136. https://doi.org/10.1021/ja00172a043
29. Sawall DD, Villahermosa RM, Lipeles RA, Hopkins AR (2004) Interfacial polymerization of polyaniline nanofibers grafted to Au surfaces. Chem Mater 16(9):1606–1608
30. Pillalamarri SK, Blum FD, Bertino MF (2005) Synthesis of polyaniline-gold nanocomposites using "grafting from" approach. Chem Commun 36:4584–4585. https://doi.org/10.1039/b419112a
31. Xing S, Tan LH, Yang M, Pan M, Lv Y, Tan Q, Yang Y, Chen H (2009) Highly controlled core/shell structures: tunable conductive polymer shells on gold nanoparticles and nanochains. J Mater Chem 19(20):3286–3291
32. Steiner AM, Mayer M, Seuss M, Nikolov S, Harris KD, Alexeev A, Kuttner C, König TAF, Fery A (2017) Macroscopic strain-induced transition from quasi-infinite gold nanoparticle chains to defined plasmonic oligomers. ACS Nano 11(9):8871–8880. https://doi.org/10.1021/acsnano.7b03087
33. Üzer A, Can Z, Akin Ii, Erçağ E, Apak R (2014) 4-Aminothiophenol functionalized gold nanoparticle-based colorimetric sensor for the determination of nitramine energetic materials. Anal Chem 86(1):351–356. https://doi.org/10.1021/ac4032725
34. Lu Y, Lam SH, Lu W, Shao L, Chow TH, Wang J (2022) All-state switching of the Mie resonance of conductive polyaniline nanospheres. Nano Lett 22(3):1406–1414. https://doi.org/10.1021/acs.nanolett.1c04969

35. Nečas D, Klapetek P (2012) Gwyddion: an open-source software for SPM data analysis. Cent Eur J Phys 10(1):181–188. https://doi.org/10.2478/s11534-011-0096-2
36. Chan MY, Leng W, Vikesland PJ (2018) Surface-enhanced Raman spectroscopy characterization of salt-induced aggregation of gold nanoparticles. ChemPhysChem 19(1):24–28. https://doi.org/10.1002/cphc.201700798
37. Ye J, Hutchison JA, Uji-i H, Hofkens J, Lagae L, Maes G, Borghs G, Van Dorpe P (2012) Excitation wavelength dependent surface enhanced Raman scattering of 4-aminothiophenol on gold nanorings. Nanoscale 4(5):1606. https://doi.org/10.1039/c2nr11805j
38. Scarabelli L, Sánchez-Iglesias A, Pérez-Juste J, Liz-Marzán LM (2015) A "Tips and tricks" practical guide to the synthesis of gold nanorods. J Phys Chem Lett 6(21):4270–4279. https://doi.org/10.1021/acs.jpclett.5b02123
39. Rossner C, König TAF, Fery A (2021) Plasmonic properties of colloidal assemblies. Adv Opt Mater 9(8):2001869. https://doi.org/10.1002/adom.202001869
40. Rohom AB, Londhe PU, Mahapatra SK, Kulkarni SK, Chaure NB (2014) Electropolymerization of polyaniline thin films. In High Performance Polymers; SAGE Publications Ltd 26:641–646. https://doi.org/10.1177/0954008314538081
41. Bhowmik KL, Deb K, Bera A, Nath RK, Saha B (2016) Charge transport through polyaniline incorporated electrically conducting functional paper. J Phys Chem C 120(11):5855–5860. https://doi.org/10.1021/acs.jpcc.5b08650
42. Patidar D, Jain N, Saxena NS, Sharma K, Sharma TP (2006) Electrical properties of CdS/polyaniline heterojunction. Braz J Phys 36:1210–1212. https://doi.org/10.1590/S0103-97332006000700016
43. Wang R, Zimmermann P, Schletz D, Hoffmann M, Probst P, Fery A, Nagel J, Rossner C (2022) Nano meets macro: furnishing the surface of polymer molds with gold-nanoparticle arrays. Nano Select 3:1502–1508. https://doi.org/10.1002/nano.202200110
44. Moon H, Lee H, Kwon J, Suh YD, Kim DK, Ha I, Yeo J, Hong S, Ko SH (2017) Ag/Au/polypyrrole core-shell nanowire network for transparent, stretchable and flexible supercapacitor in wearable energy devices. Sci Rep 7:41981. https://doi.org/10.1038/srep41981